TECHNISCHE UNIVERSITÄT
CHEMNITZ

Optimized Zone Formation in Location Dependent Resource Allocation Scheme for Device-to-Device Communication using Cluster Analysis

Master's Thesis
for
the fulfillment of the academic degree
Master of Science in Information and Communication Systems

Faculty of Electrical Engineering and Information Technology
Professorship of Communications Engineering
Prof. Dr.-Ing. Gerd Wanielik

Diplomand:	Suchith Goud Veeramalla
Matrikelnummer:	362278
Betreuer:	Dr.-Ing. Ulrich Neubert
	Mladen Botsov (BMW Forschung und Technik GmbH)
Ausgabedatum:	09.11.2015
Abgabedatum:	18.04.2016

Selbständigkeitserklärung

Hiermit versichere ich, dass ich die vorliegende Masterarbeit mit dem Thema "Optimized Zone Formation in Location Dependent Resource Allocation Scheme for Device-to-Device Communication using Cluster Analysis" selbständig verfasst und keine anderen als die angegebenen Quellen und Hilfsmittel verwendet habe. Weiter erkläre ich wörtliche und sinngemäße Zitate als solche gekennzeichnet zu haben.

Ort, Datum

Suchith Goud, Veeramalla

Vorname, Name

Unterschrift

Abstract

Device-to-device communication introduced in LTE Release 12 seems to be a potential paradigm for the V2V communication. Anticipating the potential benefits of D2D communication paradigm for the V2V services, Location Dependent Resource Allocation Scheme (LDRAS) was developed. In this scheme, each cell is divided into disjoint zones where in each zone a set of resource blocks are dedicated for D2D communication and the same set of resorce blocks are reused by the cellular user terminals within the cellular network in different zones which are spatially well seperated to guarantee the minimum SINR. Thus, the zone design plays an important role in this scheme. In this thesis, a formal definition for the zone design which constitutes a multi-dimensional trade-off spanning the domains of the SIR targets for the D2D communication and the cellular communication, the power of vehicle user terminals and cellular user terminals, the spatial separation between the D2D receiver and the interfering cellular terminals and between eNodeB and the interfering D2D transmitter is introduced. As a part of this, two optimization problems are formulated which maximizes the number of zones which eventually improves resource utilization by providing increased oppurtunities for reuse. As LDRAS depends on the deployment environment, an environment that constitutes different propagation topologies and channel conditions is created and a framework which utilizes the optimal values obtained in the optimization problems in constructing a dataset which is used to determine the zone layout in the considered environment using cluster analysis is developed. Finally, results for the two optimization problems and the optimized zone formations in an isolated sector and LTE following $1 \times 3 \times 1$ reuse pattern where one cell site has three sectors and using same frequency set are studied using MATLAB.

Acknowledgments

I would like to thank my mentor Dr.-Ing. Ulrich Neubert for his support and encouragement during my thesis, especially for his advices when I had difficulty in choosing the offered topic. I would also like to thank him for his lessons in the last two years which has given me a different outlook towards learning. I would express my heartfelt gratitude to my advisor Mladen Botsov for his constant support, encouragement, patience and prompt response throughout my thesis and appreciate his willingness to help me on his tight schedule. I would extend my thanks to my professor Dr.-Ing. Gerd Wanielik whose lessons in the last two years and ideas too inspired me in taking a different approach towards learning.

I would also like to thank my parents who worked hard in bringing us up and to provide us a better future. I would specially thank my sister, brother-in-law, brother and aunt for their encouragement and moral support I have received in my life. Finally, I would like to thank my friends who supported me at crucial times.

Contents

3.2 Convex Optimization

The optimization problem (3.3) is convex if the objective function f_0 is convex, the functions $g_i : \mathbb{R}^n \to \mathbb{R}$, $i = 1, \ldots, m$, are convex and $h_i : \mathbb{R}^n \to \mathbb{R}$, $i = 1, \ldots, n$, are affine. Formally, for the following optimization problem

$$\begin{array}{ll} \underset{x}{\text{minimize}} & f_0(x) \\ \text{subject to} & f_i(x) \leq b_i,\ i = 1, \ldots, m, \end{array} \tag{3.4}$$

the functions $f_0, \ldots, f_m$ satisfy

$$f_i(\alpha x + \beta y) \leq \alpha f_i(x) + \beta f_i(x)$$

$\forall\, x, y \in \operatorname{dom} f$ and all $\alpha, \beta \in \mathbb{R}$ with $\alpha + \beta = 1$, $\alpha \geq 0, \beta \geq 0$ and dom f is a convex set [BV04]. We can test for convexity of a function using the following conditions.

3.2.1 First-order conditions

Suppose a function f is differentiable (i.e. its gradient ∇f exists at each point in dom f), then f is convex if and only if dom f is convex and

$$f(y) \geq f(x) + \nabla f(x)^T (y - x)$$

holds $\forall\, x, y \in \operatorname{dom} \dot{f}$ [BV04].

3.2.2 Second-order conditions

Suppose a function f is twice differentiable (i.e. its *Hessian* or second derivative $\nabla^2 f$ exists at each point in dom f), then f is convex if and only if dom f is convex and its Hessian is positive semidefinite [BV04]:$\forall\, x, y \in \operatorname{dom} f$,

$$\nabla^2 f(x) \geq 0$$

For a function on $\mathbb{R}$, this condition simply reduces to $f''(x) \geq 0$ which means that the derivative is nondecreasing [BV04]. Similarly, f is concave if and only if dom f is convex and $\nabla^2 f(x) \leq 0\ \forall\, x, y \in \operatorname{dom} f$ [BV04]. We use the above conditions to check if our optimization problems defined in Section (3.4) is convex.

3.3 Taxonomy of Problem Formulation

3.3.1 Basic System Model

At this juncture, it is important to understand the derivation for the two equations outlined in previous sections. Consider the system model and parameters introduced in previous chapter. We know that SIR of a communication link utilizing particular radio resources can be given as

$$SIR = \frac{P}{I}$$

where P denotes the power of the desired signal in linear scale and I denotes the power of the interference signal in linear scale. In dB scale, the SIR can be written as

$$SIR_{\mathrm{dB}} = P_{\mathrm{dB}} - I_{\mathrm{dB}}$$

where $P_{\mathrm{dB}} = 10\log_{10} P$ is the power of desired signal expressed in dB and $I_{\mathrm{dB}} = 10\log_{10} I$ is the power of interference signal in dB.

3.3.2 Derivation for r_1

In the beginning of the chapter, consider the inequality (3.1) which reflects the conditions for reliable cellular communication. In this manner, the power of signal transmitted by cellular user terminal can be expressed as the targeted Received Signal Strength (RSS) at the eNodeB imposed by UL power control which is given by [Bot13],

$$P_{\mathrm{dB}} = R_0.$$

Here, the interference signal is the signal transmitted by a vehicular user terminal reusing the same UL radio resources as the considered cellular user terminal. Hence, ignoring the fading effects, the interference power experienced by the cellular user terminal can be expressed as the product of power of interfering vehicular user equipment and the distance dependent path loss. However, in dB scale, it can be expressed as the difference between the transmit power of the V-UE $P_{\text{V-UE}}$ (in dB) and the distance dependent path loss of the signal $pl(r_1)$ (in dB). Considering the maximum antenna gain G_0(in dB), the interference signal in the worst case scenario can be expressed as [Bot13]

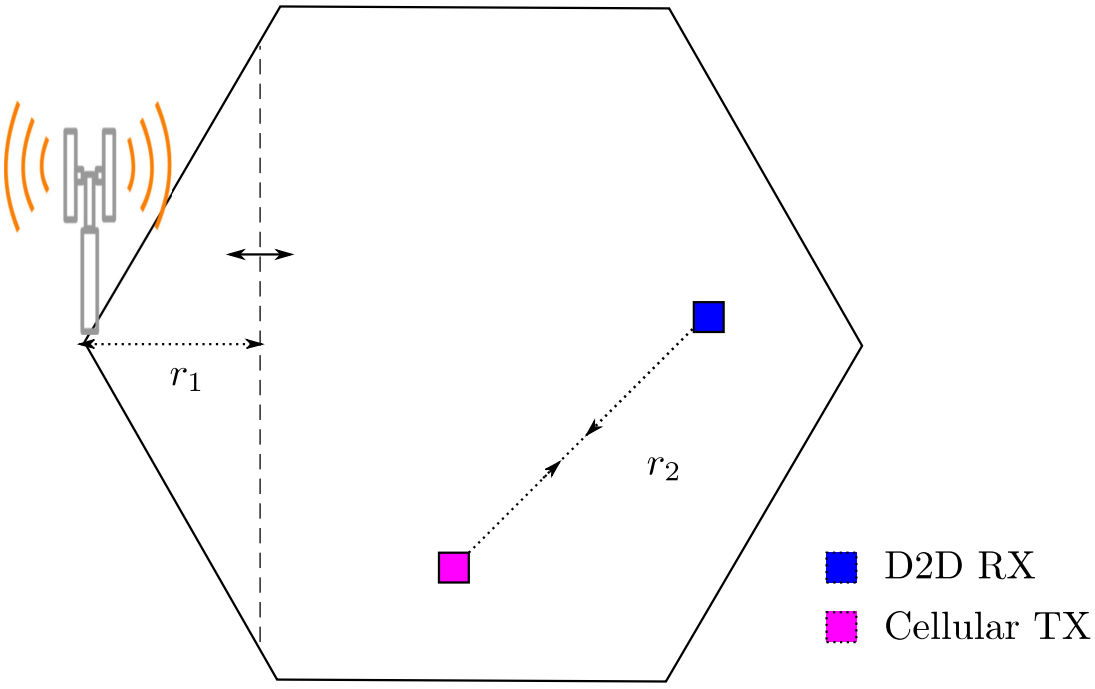

Figure 3.1: Idea of our objective of maximizing the reuse efficiency

3.3.5 Objectives

In this work, the main goal is to formulate the optimization problem with an objective to maximize the number of zones and consequently the reuse efficiency. We approach the problem of constructing the optimization problem through r_1 and r_2 as they play a vital role in zone design. Indeed, they are considered as the zone design parameters. We are already familiar with r_1 where dedicated resources for D2D communication are not reused in the cellular network and remaining part of the cell or a sector where the resources assigned for D2D communication are reused in the primary network at certain distance r_2. We might consider shrinking r_1. In this manner, the number of RB sets assigned to this zone can be reduced as the size of the RB sets is proportional to the size of the zone. Consequently, this will increase the number of RBs for reuse in the remaining part of the cell or a sector. Simultaneously, we might also consider to reduce r_2 as r_1 and r_2 have opposite effects on our optimization variable ($P_{\text{V-UE}}$) which is illustrated in Figure 3.2. In this manner, we hope to maximize the number of zones. Figure 3.1 illustrates the basic idea of our objective of maximizing the number of zones. As a part of this work, in this thesis two optimization problems are formulated which are defined in Section 3.4.

3.4.2 Nonlinear Fractional Programming

The fractional programming problem takes the form [RLV99]

$$\max_{x} \quad f_0(x) = \frac{g(x)}{h(x)} \tag{3.18}$$

where $x \in X$ and X is a compact and connected set of $\mathbb{R}$. The functions $g(x)$ and $h(x)$ are continuous and real-valued functions of $x \in X$. In addition, the following assumption is also made:

$$h(x) > 0, \qquad \forall\, x \in X$$

One of the well-known methods under this class is Dinkelbach's algorithm [Din67]. However, the numerator $(R - r1)$ and the denominator (r_2) of the functions should be concave and convex or convex and concave respectively over the convex set in which our optimization variable P_{V-UE} is constrained. To solve our optimization problem using this technique, we shall check if the objective function satisfies the assumptions made by Dinkelbach.

Check for Convexity

We begin by considering the equation for r_1. To prove if the Equation (3.9) which is derived in Section 3.3 is convex, we follow the second order conditions mentioned in Section 3.2. Since the Equation (3.9) is defined on $\mathbb{R}$ with variable $P_{\text{V-UE}}$, we simply check if $r_1''(P_{\text{V-UE}}) > 0$. The equation is given by,

$$r_1 = 10^{\left(\frac{\gamma_c - R_0 + P_{\text{V-UE}} + G_0 - B + I_{\text{dB}}^{\text{eNodeB}}}{A}\right)}$$

Since, γ_c, R_0, G_0, $I_{\text{dB}}^{\text{eNodeB}}$ are constants, the right-hand side (RHS) of the equation can be written as

$$r_1 = 10^{\left(\frac{T + P_{\text{V-UE}}}{A}\right)}$$

Finally, replacing the fractional part by $\tilde{P}_{\text{V-UE}}$, the equation can be written as

$$r_1(\tilde{P}_{\text{V-UE}}) = 10^{\tilde{P}_{\text{V-UE}}}$$

and non-linear parametric programming which forms the base of this algorithm has been given with the following problem [Jag66] [Din67]

$$\Phi(q) = \max_{x} \qquad g(x) - q \cdot h(x), x \in X \tag{3.19}$$

where

$$q = f_0(y)$$

$\forall\, y \in X$ is the objective function in optimization problem (3.18)

Theorem 3.4.1 *Let $y \in X$, y is an optimal solution for the problem (3.18) if and only if y is an optimal solution for*

$$\max_{x} \qquad g(x) - f_0(y) \cdot h(x), x \in X$$

The problem (3.19) has a solution for any $q \in \mathbb{R}$ as X is a compact set of $\mathbb{R}^n$ and g and h are continuous on X [Din67] [RLV99].

Lemma 3.4.2

$$\Phi(q) = \max_{x} \qquad g(x) - q_k \cdot h(x), x \in X \textit{is convex}$$

As already mentioned, Dinkelbach [Din67] developed a method for solving nonlinear fractional problems by assuming the function g as concave and h as convex. The steps involved in this algorithm are given by,

Step 1

Let x_1 be initial feasible guess within the set X and $q_k = f(x_k)$. In this manner, for $k = 1$, $q_1 = f(x_1)$.

Step 2

Now consider the following subproblem which is already stated previously.

$$\Phi(q_k) = \max_{x} \qquad g(x) - q_k \cdot h(x), x \in X \tag{3.20}$$

As stated in Lemma 3.4.2, the above problem is convex and can be solved by any convex optimization technique. In this thesis we go by one of the Interior-Point methods [BV04] briefed out in the next section. Let the new solution after solving the above subproblem be denoted as x_{k+1}

Step 3

If $\Phi(q_k)$ is 0, then x_k is the solution for the problem. Otherwise, repeat Step 2 by setting $q_{k+1} = f_0(x_{k+1})$ and $k = k + 1$.

It should be noted that the above theorem is also valid for minimization problems. In addition, the algorithm is valid for general fractional problem where the subproblem (3.20) generated in all iterations are not necessarily convex [RLV99]. The algorithm described above steps converges after a finite number of iterations in linear problems, but this is not necessarily true for the nonlinear case [Din67].

Theorem 3.4.3 *[RLV99] Dinkelbach's algorithm either terminates in a finite number of iterations or it generates an infinite sequence so that any accumulation point solves the problem (3.20).*

Lemma 3.4.4 *[RLV99]*

$$\Phi(q) = \max_{x} \quad g(x) - q_k \cdot h(x), x \in X \textit{is strictly monotonic decreasing}$$

Lemma 3.4.5 *[RLV99] Assume that x_k is a feasible point in (3.18) and x_{k+1} solves the subproblem (3.20). If x_k solves the subproblem (3.20), then x_k is an optimal solution in (3.18). If not, $q_{k+1} < q_k$*

Therefore, in this thesis, Dinkelbach's truncated algorithm [RLV99] is employed where the number of iterations (n_k) is limited. However, the optimal solution obtained by limiting the number of iterations can be justified by the Lemma 3.4.4 and Lemma 3.4.5.

3.4.4 Interior-Point Methods

In order to solve our optimization problems, one of the interior-point methods is employed in this thesis. These methods are more popular in the mathematical community and are applicable to all nonlinear optimization problems irrespective of convexity or concavity [BV04] [NT08]. However, small modifications exists in solving both kinds of problems (i.e. convex and nonconvex), for example, choosing step size with respect to a merit function (3.35). In this section, the working principle of primal-dual interior point algorithm based on line searches [BV04] [BVS02] is explained. In such methods, the search directions are obtained using Newton's method [BV04], applied to the modified KKT equations [BV04].

Let us consider an optimization problem given below

$$\begin{aligned} \underset{x}{\text{minimize}} \quad & f_0(x) \\ \text{subject to} \quad & g_i(x) \leq 0,\ i = 1, \ldots, m. \end{aligned} \tag{3.21}$$

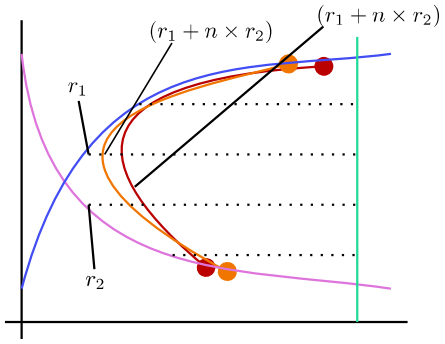

Figure 3.5: Feasible region of the optimization problem (3.36) with the objective function taking one of the forms

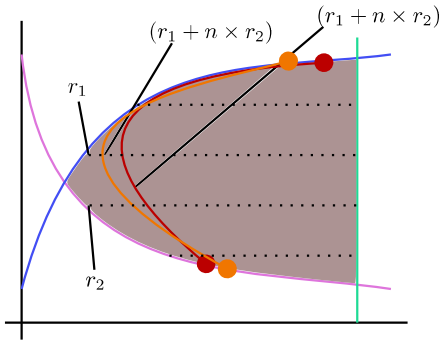

Figure 3.6: Feasible region after nonlinear relaxation with the objective function taking one of the forms

achieved by adding a valid inequality that is satisfied by all feasible solutions to the MINLP to the relaxation.

In branching, we partition the feasible set into smaller and smaller subsets such that a feasible solution is possible in any one of the subset. When the integrality constraint is relaxed, the subsets are allowed to branch on an integer variable that takes a fractional value x'. In this manner, the branching creates two subproblems with separate relaxations. The constraint set $x \leq \lfloor x' \rfloor$ is added to the first subproblem and the constraint set $x \geq \lceil x' \rceil$ is added to the other [BKL+13]. These resulting subproblems are organized in a search tree to keep track of all the subproblems that have to be solved. This principle forms the basis for the branch-and-bound technique explained in next subsection.

Consider Figure 3.7 which illustates the feasible region of the nonlinear function obtained by relaxing the integrality constraints in our optimization problem. Suppose, we have a solution $(P'_{\text{V-UE}}, n')$ represented by a black dot in the figure after solving the NLP problem (i.e. the optimization problem after relaxing the integrality constraints). We know that the variable $P_{\text{V-UE}}$ can take any continuous value within the constrained set. So, it will be within the feasible region of the original problem de-

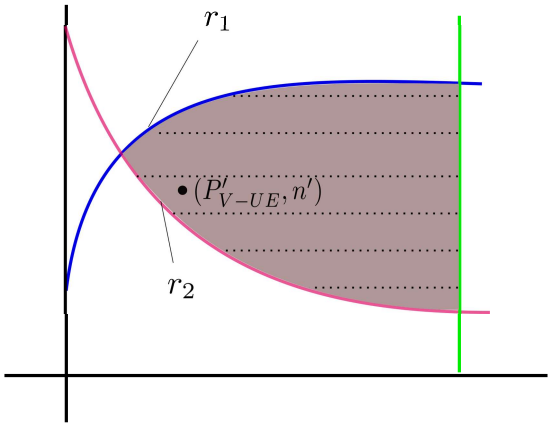

Figure 3.7: Feasible region after nonlinear relaxation

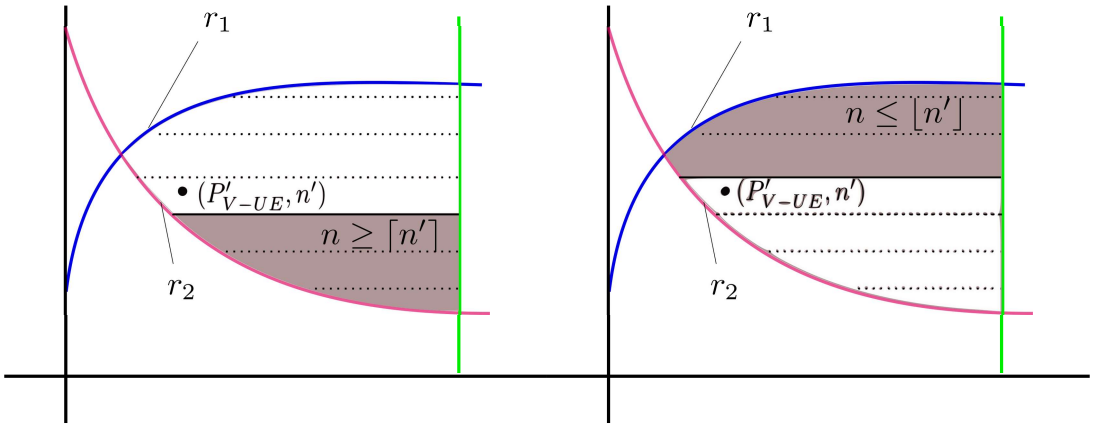

(a) Branching on $n \geq \lceil n' \rceil$ (b) Branching on $n \leq \lfloor n' \rfloor$

Figure 3.8: Branching on the integer variable n

fined. However, the value of n' in Figure 3.7 is not feasible to the original problem as it is allowed to take only integer values. Now, we branch on this continuous variable which eventually creates two subproblems with two separate relaxations as shown in Figure 3.8. In this manner, we eliminate the infeasible point (i.e. the solution represented by black dot).

3.4.8 Branch-and-Bound Method

Initially, we start the algorithm by relaxing the integrality constraints on the integer variables x_i, $i \in Z^+$ in the optimization problem (3.39) and solve it by any one of the nonlinear programming methods. In this monograph, we use interior-points method explained in Section 3.4.4 to solve the resulting optimization problem after relaxing

the integrality constraints. The branch-and-bound technique is based on single-tree method and hence we start explaining this algorithm using the corresponding terminology. In this manner, we define the resulting optimization problem after relaxing the integrality constraints as root node. We begin by checking the feasibility of relaxation in the first step. If the relaxation is infeasible, then the MINLP is also infeasible. If we have an integer solution say for the optimization problem after relaxation, then solving MINLP is feasible. If not, then we define another node that correspond to NLP subproblem and each edge correspond to branching decisions. In this manner a tree is constructed which is illustrated in Figure 3.9 and branch-and-bound searches this tree when there is no integer solution after relaxation. We define each node by the following optimization problem [BKL+13]:

$$\begin{aligned} \underset{x}{\text{minimize}} \quad & f_0(x) \\ \text{subject to} \quad & g_i(x) \leq R_1, \\ & x \in X, \\ & l_i \leq x_i \leq u_i, \forall i \in Z^+ \end{aligned} \tag{3.40}$$

where the bounds on integer variables for corresponding NLP are set to (l_i, u_i). We formally describe the branching in the following section.

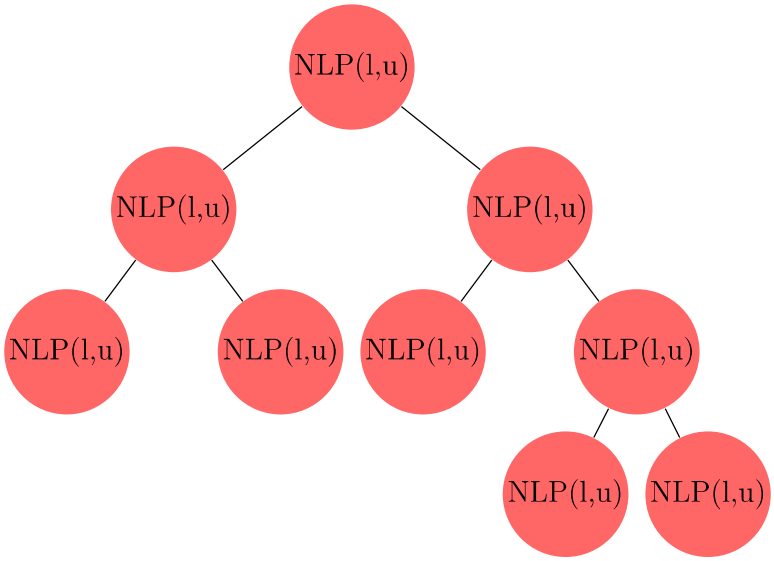

Figure 3.9: Tree in Branch-and-bound

Branching

Consider the optimization problem (3.40) given above. Let us represent the optimization problem as NLP(l,u). If the solution after solving NLP(l, u) is x' and if it is not

Chapter 4

Zone formation using Cluster Analysis

4.1 Introduction

In the previous chapter, we have seen two mathematical formulations which give us the optimized power value under the objective of improving the reuse efficiency. In short, we have defined a formal model which gives us the operating value of power of vehicle user terminal ($P_{\text{V-UE}}$) as opposed to definition by intuition in previous work.

In real time, path-loss for each receiving terminal is inconsistent. We have to consider NLOS scenarios in addition to LOS and the underlying fading characteristics in determining the zones. The zones can take any arbitrary rectangular shape in 2-D and the optimization problem we solved does not envisage the formation of zones with capricious rectangular shape. This chapter deals with developing a model for the zone formation in such an uncompromising environment.

4.2 Motivation

While formulating an optimization problem in such tough environments, different channel models and fading characteristics need to be considered. In addition, we need to consider different propagation topologies: Outdoor-to-Outdoor (O2O), Outdoor-to-Indoor (O2I), Indoor-to-Outdoor (I2O) and Indoor and different environments: Dense Urban, Urban, Suburban, Highway and Rural. Thus, it becomes a difficult task to derive and formulate an optimization problem incorporating these facts.

Moreover, new technologies are evolving rapidly. Therefore, 5G networks might see

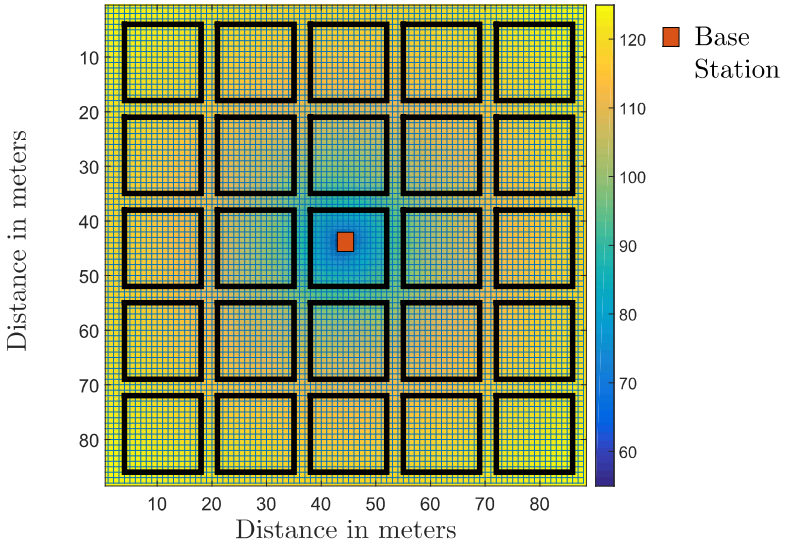

Figure 4.3: The path loss in dB experienced by the C-UEs in the urban macrocell

streets in the coverage area as "the main street", "perpendicular streets" and "parallel streets" [KSB+07].

In the main street, there is a LOS from all locations to the user equipment transmitter. However, there are few exceptions in cases where the LOS is temporarily blocked by traffic (e.g. trucks and buses) on the street. The streets that intersect the main street are referred to as perpendicular streets, and the streets that run parallel to it are referred to as parallel streets. The desired signal reaches the user terminals in NLOS streets as a result of the propagation around corners and through buildings. In this manner, we shall calculate path loss for each D2D TX-RX pair differentiating between LOS and NLOS. The corresponding path loss equations for LOS and NLOS computed (by considering the system parameters in Chapter 5) according to Winner+ [JK+10] are given by,

$$PL(a^{(ij)}) = \begin{cases} 40\log_{10}(a^{(ij)}) + 17.7, & \text{LOS} \\ min(PL(a_1^{(ij)}, a_2^{(ij)}), PL(a_2^{(ij)}, a_1^{(ij)})) & \text{NLOS} \end{cases} \tag{4.3}$$

where

$$PL(a_k^{(ij)}, a_l^{(ij)}) = 40\log_{10}(a^{(ij)}) + 17.71 + 17.00 - 12.5n_p + 10n_p\log_{10}(a_l^{(ij)})$$

and

$$n_p = max(2.8 - 0.0024a_k^{(ij)}, 1.84) \text{ and } k, l \in \{1, 2\}$$

and

$$a_{k,l}^{(ij)} = \sqrt{(x_{\text{dt}}^{(i)} - x_{\text{dr}}^{(j)})^2 - (y_{\text{dt}}^{(i)} - y_{\text{dr}}^{(j)})^2}$$

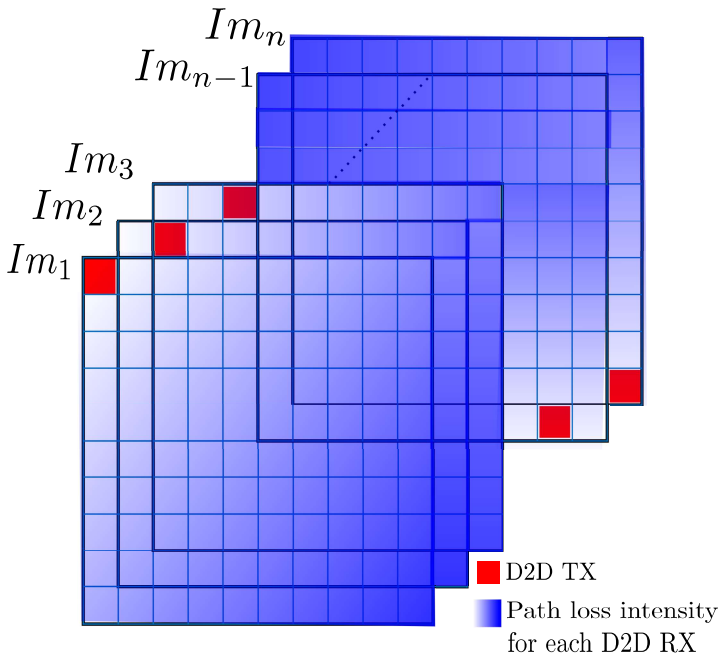

Figure 4.5: Set of images formed by placing the D2D transmitter at all the pixel locations in the map

Thus, we will have a set of 2-D matrices which represents the path loss values.

O2I, I2O and Indoor

When it comes to indoor to outdoor, i.e. when a D2D transmitter is within building, we shall differentiate between the receivers within a building and the outdoor receivers. Here, we shall consider the streets adjacent to the building as LOS and apply the two path loss models for the distance from a nearest wall to the transmitter to the outdoor and for the distance from the transmitter location to this nearest wall. In the former case, we apply the path loss for urban microcell in O2O scenario while in the latter, we consider the path loss formula for indoor scenarios. Similarly, we shall calculate the path loss for the outdoor to indoor case. Figure 4.6 and Figure 4.7 illustrates the path loss in dB experienced by all the D2D receivers at different pixel locations in the D2D layer when a D2D transmitter is located inside a building and in a street respectively. It is also worth noting that the path loss for the parallel streets corresponding to the street where the D2D transmitter is located are not computed (Figure 4.7). The path loss equations computed according to Winner [KSB+07] and 3GPP [3GP14] are given by

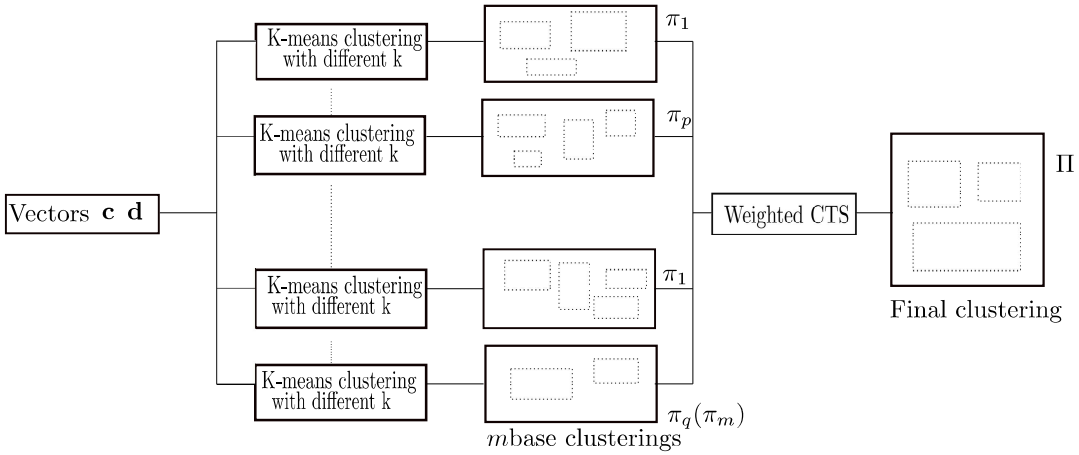

Figure 4.13: Ensemble clustering

sent the actors and the edges a tie between these actors. In bibliographical terms, we say the actors as the authors. Clustering describes a circumstance that if one author is connected or has a tie to two other authors, then the two other authors are also likely to have a tie [KRW+06]. This can be described by a simple analogy. Consider one has a group of friends and the other has a group of friends. These both sets are likely to have an overlap between them. The authors in multi-mode networks might be connected in other ways considering single publications, conferences, journals. Consider a relationship "coauthors of coauthors" within bibliographical data. In this context, the clustering describes that if two not collaborating authors are connected to a third author, then there is likely that they get to know each other. In this case the three authors are each connected by a tie and form a triangle in the network. In this way, a triangle $\triangle = (V, E)$ can be described as a subgraph of G consisting of three vertices with $V_\triangle = \{V_1, V_2, V_3\} \subset V$ and $E = \{(e_{V_1}, e_{V_2}), (e_{V_2}, e_{V_3}), (e_{V_3}, e_{V_1})\} \subset E$ [KRW+06]. Consider the other case where the two not collaborating authors are not connected. In that case, there exists no tie between the two not collaborating authors and a connected triple occurs between these authors. A Connected Triple $\wedge = \{V_\wedge, E_\wedge\}$ can be described as a subgraph of Gr consisting of three vertices with $V_\wedge = \{V_1, V_2, V_3\} \subset V$ and $E_\wedge = \{(e_{V_1}, e_{V_2}), (e_{V_1}, e_{V_3})\} \subset E$. The author connecting the two not collaborated authors is called center of the connected triple [KRW+06]. Generally, we can say that a triple $\wedge = (V_\wedge, E_\wedge)$, is a subgraph of Gr consisting of three vertices $V_\wedge = \{v_x, v_y, v_k\} \subset V$ and two edges $E_\wedge = \{e_{x_k}, e_{y_k}\} \subset E$. It should be noted that $e_{xy} \notin E$.

To illustrate this in our terms, let us consider a set of receivers $X = \{x_1, \ldots, x_n\}$. Now, we perform K-means on these receivers with random initializations and different number of zones for m times. This results in m base clusterings $(\pi_1 \ldots \pi_m)$. Formally, there will be a tie between a receiver x_i and cluster G_j^m if x_i belongs to G_j^m within the base clustering. From the Figure 4.15, it can be inferred that x_1 and x_2 are similar with respect to the clustering results π_2 and π_3 despite being assigned to two

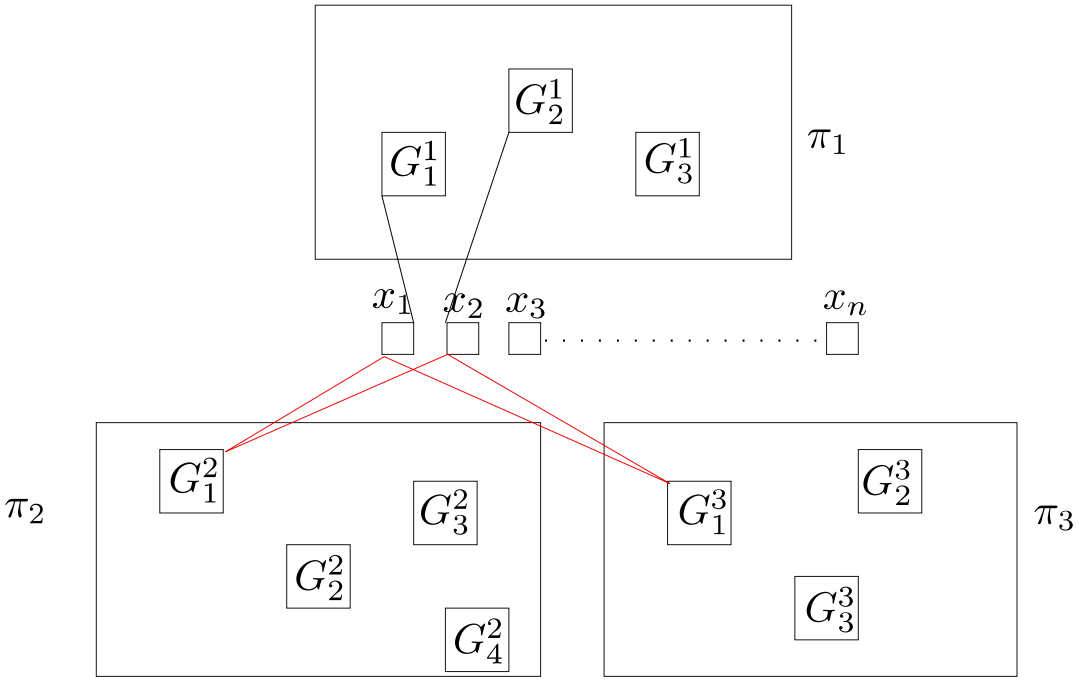

Figure 4.14: Connected-Triple algorithm

different clusterings. In this example, using connected triple technique, cluster G_1^1 and G_2^2 are considered to be similar as they possess 2 connected-triples (represented by red lines in Figure 4.14) with cluster G_1^2 and G_1^3 as centers of the triples. In this way, the similarities are judged based on the number of triples associated with any two receivers. However, the similarity matrix is more efficiently carried out by Weighted connected-triple algorithm (WCT) [IoG$^+$10] which also considers the characteristics of shared data members among the clusters.

Weighted connected-triple algorithm

If V represents a set of vertices each representing a cluster in Π and W represents a set of weighted edges between these clusters, then a graph $Gr = (V, W)$ can be constructed from a cluster ensemble Π of a set of data points X. Formally,the weight of the edge w_{ij} which connects two clusters $G_i, G_j \in V$ is estimated by the fraction of overlayed points. In this manner the equation for w_{ij} is given by [IoG$^+$10]

$$w_{ij} = \frac{|X_{G_i} \cap X_{G_j}|}{|X_{G_j} \cup X_{G_j}|} \tag{4.16}$$

where $X_{G_i} \subset X$ denotes the set of data points that belong to cluster G_i. In this method each triple is regarded as minimum weight of the two considered edges.

Variables / γ_d (dB)	r_1 (m)	r_2 (m)	$P_{\text{V-UE}}$ (dBm)	n
1	113	149.1	-9.9	5.2
2	120.3	148.9	-8.9	5.1
3	128.4	147.9	-7.8	5.1
4	137.1	147.0	-6.7	5.0
5	145.2	147.3	-5.7	5.0
6	154.0	147.3	-4.7	4.9
7	163.3	147.4	-3.7	4.9
8	172.6	147.9	-2.8	4.8

(a) With relaxation

Variables / γ_d (dB)	r_1 (m)	r_2 (m)	$P_{\text{V-UE}}$ (dBm)	n
1	114.9	147.0	-9.7	5
2	117.3	152.5	-9.3	5
3	125.9	150.8	-8.1	5
4	135.3	148.9	-6.9	5
5	145.5	147.0	-5.7	5
6	118.3	190.4	-9.1	4
7	127.0	188.2	-7.9	4
8	136.5	185.9	-6.7	4

(b) Without relaxation

Table 5.2: Results for OP_2 with and without relaxation of the integrality constraint for $\gamma_c = 7$ dB in an isolated sector

Variables / γ_d (dB)	r_1 (m)	r_2 (m)	$P_{\text{V-UE}}$ (dBm)	n
1	219.9	160.8	-3.4	4.1
2	219.6	170.4	-3.4	3.9
3	219.7	180.4	-3.4	3.7
4	219.6	191.6	-3.5	3.4
5	219.5	202.9	-3.5	3.3
6	219.8	216.9	-3.6	3.1
7	219.6	228.4	-3.5	2.9
8	219.6	241.5	-3.5	2.7

(a) With relaxation

Variables / γ_d (dB)	r_1 (m)	r_2 (m)	$P_{\text{V-UE}}$ (dBm)	n
1	211.4	167.2	-4.1	4
2	153.3	242.2	-9.5	3
3	165.4	238.2	-8.3	3
4	178.9	233.7	-6.9	3
5	194.1	228.6	-5.5	3
6	211.4	222.9	-4.1	3
7	220.0	227.1	-3.4	3
8	220.0	240.5	-3.4	3

(b) Without relaxation

Table 5.3: Results for OP_2 with and without relaxation of the integrality constraint for $\gamma_c = 7$ dB in a $1 \times 3 \times 1$ reuse pattern

Variables / γ_d (dB)	r_1 (m)	r_2 (m)	$P_{\text{V-UE}}$ (dBm)	n
1	136.6	147.6	-9.7	5.0
2	143.8	148.7	-8.8	5.0
3	141.9	159.5	-9.1	4.6
4	163.6	147.1	-6.7	4.9
5	173.4	147.2	-5.7	4.8
6	183.9	147.3	-4.7	4.7
7	195.0	147.3	-3.7	4.6
8	206.7	147.4	-2.7	4.6

(a) With relaxation

Variables / γ_d (dB)	r_1 (m)	r_2 (m)	$P_{\text{V-UE}}$ (dBm)	n
1	135.3	148.9	-9.9	5.0
2	145.5	147.0	-8.7	5.0
3	154.3	147.0	-7.7	5.0
4	163.7	147.0	-6.7	5.0
5	136.5	185.9	-9.7	4.0
6	146.9	183.3	-8.5	4.0
7	158.4	180.4	-7.2	4.0
8	171.1	177.2	-5.9	4.0

(b) Without relaxation

Table 5.4: Results for OP_2 with and without relaxation of the integrality constraint for $\gamma_c = 10$ dB in an isolated sector

Variables / γ_d (dB)	r_1 (m)	r_2 (m)	$P_{\text{V-UE}}$ (dBm)	n
1	219.9	191.1	-6.4	3.5
2	219.9	202.5	-6.4	3.3
3	219.7	214.6	-6.4	3.1
4	219.6	227.5	-6.5	2.9
5	219.2	241.4	-6.5	2.7
6	219.3	255.5	-6.5	2.6
7	220.0	269.9	-6.4	2.4
8	220.0	285.9	-6.4	2.3

(a) With relaxation

Variables / γ_d (dB)	r_1 (m)	r_2 (m)	$P_{\text{V-UE}}$ (dBm)	n
1	178.9	233.7	-9.9	3.0
2	194.1	228.6	-8.5	3.0
3	211.4	222.9	-7.1	3.0
4	220.0	227.1	-6.4	3.0
5	220.0	240.5	-6.4	3.0
6	220.0	254.8	-6.4	3.0
7	220.0	269.9	-6.4	3.0
8	178.3	350.8	-10.0	2.0

(b) Without relaxation

Table 5.5: Results for OP_2 with and without relaxation of the integrality constraint for $\gamma_c = 10$ dB in a $1 \times 3 \times 1$ reuse pattern

Results for OP_1

Here, the results for OP_1 are tabulated in an isolated sector and $1 \times 3 \times 1$ frequency reuse pattern of a LTE system for $\gamma_c = 7$ dB.

Variables / γ_d (dB)	r_1 (m)	r_2 (m)	$P_{\text{V-UE}}$ (dBm)	n
1	114.9	147.0	-9.7	5.2
2	121.9	147.0	-8.7	5.2
3	129.3	147.0	-7.7	5.1
4	137.1	147.0	-6.7	5.1
5	145.5	147.0	-5.7	5.0
6	154.3	147.0	-4.7	4.9
7	163.7	147.0	-3.7	4.9
8	173.7	147.0	-2.7	4.8

(a) Isolated sector

Variables / γ_d (dB)	r_1 (m)	r_2 (m)	$P_{\text{V-UE}}$ (dBm)	n
1	220.0	160.8	-3.4	4.1
2	220.0	170.3	-3.4	3.9
3	220.0	180.4	-3.4	3.7
4	220.0	191.1	-3.4	3.5
5	220.0	202.4	-3.4	3.3
6	220.0	214.4	-3.4	3.1
7	220.0	227.1	-3.4	2.9
8	220.0	240.5	-3.4	2.7

(b) $1 \times 3 \times 1$ reuse pattern

Table 5.6: Results for OP_1 for $\gamma_c = 7$ dB in an isolated sector and $1 \times 3 \times 1$ reuse pattern

5.2.2 Comparison of the results

In this subsection, we begin by studying the results for OP_1. Then, we see how the results of OP_1 differ from the results of OP_2. Finally, we study the results for OP_2 without relaxing the integrality constraint which is the primary objective of its formulation and compare the results for an isolated cell sector and for a cell following $1 \times 3 \times 1$ reuse pattern.

Let us consider the results for OP_1 . Looking at Figure 5.1 (b), we see that the $P_{\text{V-UE}}$ in the isolated sector constantly increases with increasing γ_d as expected. However, the variable $P_{\text{V-UE}}$ in this case is influenced by the lower bound on r_2. This is because the least possible value for r_2 within the feasible set of the optimization problem for the considered path loss equation lies around 50 m (Figure 3.2 (b)) and the constraint set on r_2 is 147 m. This mean that relaxing the constraint on r_2 in the optimization problem would yield r_2 value that can be lower than the lower bound on r_2. Thus, in this case we see that the values of r_2 (shown by a line in Figure 5.1 (a)) for the considered values of γ_d are equal to R_2. Analogously, the variable $P_{\text{V-UE}}$ in a cell following $1 \times 3 \times 1$ reuse pattern is influenced by the upper bound on r_1 as in this case, the upper bound of r_1 is dominated over the lower bound on r_2 and hence we see the value of $P_{\text{V-UE}}$ is constant irrespective of changing values of γ_d.

However, these trends are observed for the path loss models considered in this thesis

r_1	136.5 m
r_2	185.9 m
$P_{\text{V-UE}}$	-6.7 dBm
γ_d	8 dB
γ_c	7 dB
Th_{D2D}	86.3 dB
Th_{I}	108.4 dB
Th_{C}	99 dB
n	4
k	11 - 15

Table 5.7: Values for the zone formation in the isolated sector using results for OP_2

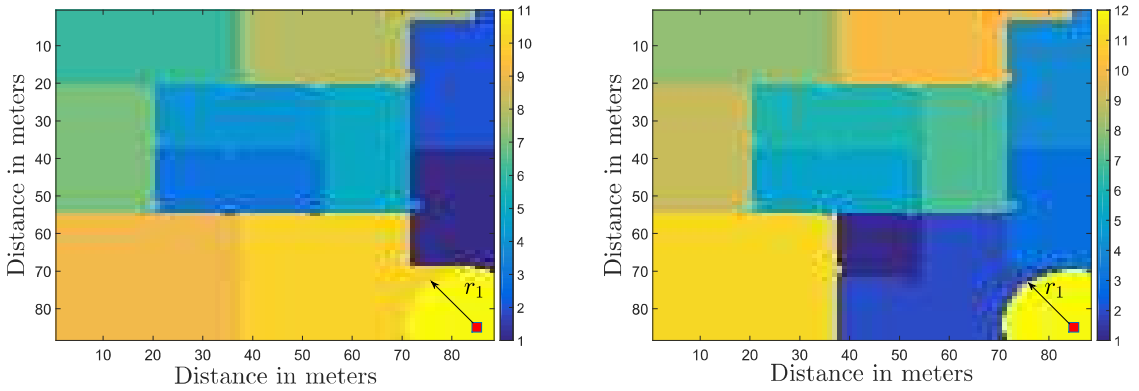

(a) $k = 11$ (b) $k = 12$

(c) $k = 13$ (d) $k = 15$

Figure 5.5: Zone formations for different k in an isolated sector using the results for OP_2